Appl. Phys. A
DOI 10.1007/s00339-014-8348-9

Applied Physics A
Materials Science & Processing

Leakage current analysis of $La_{0.67}Sr_{0.33}MnO_3$/Nb:$SrTiO_3$ p–n junctions

R. K. Pan · Z. C. Xia · Y. B. He · M. K. Li · P. Li · P. K. Liu

Received: 22 January 2014 / Accepted: 23 February 2014

Abstract $La_{0.67}Sr_{0.33}MnO_3$ (LSMO) films were grown on 0.7 wt% Nb-doped $SrTiO_3$ (NSTO) single-crystal substrates by pulsed laser deposition. The crystal phase structure and surface morphology of the LSMO films were investigated by means of X-ray diffraction method and atomic force microscopy, respectively. The diode-like behavior was observed in the leakage currents of the LSMO/NSTO heterojunction, by which *I–V* curves were measured at room temperature. The leakage current of LSMO/NSTO heterojunction follows the space-charge-limited conduction (SCLC) model under lower forward bias. As the forward bias increases, the barrier at the LSMO/NSTO interface becomes narrower and lower, which allows electrons to go over/through the interface barrier by the conduction mechanisms of Schottky emission and interface-limited Fowler–Nordheim tunneling, respectively. Under the same backward bias, the leakage current still undergoes the Ohmic law region according to the SCLC model, which is due to the drift currents of holes in the LSMO films and electrons in the NSTO substrates.

R. K. Pan (✉) · Y. B. He · M. K. Li · P. Li · P. K. Liu
School of Materials Science & Engineering, Hubei University, Wuhan 430062, People's Republic of China
e-mail: panruikun5@hotmail.com

R. K. Pan · Z. C. Xia
Wuhan National High Magnetic Field Center, Huazhong University of Science and Technology, Wuhan 430074, People's Republic of China
e-mail: xia9020@hust.edu.cn

1 Introduction

Perovskite-like doped lanthanum manganite $La_xSr_{1-x}MnO_3$ films are often used as ferromagnetic layer in spin tunnel junctions, magnetoelectric effect and multiferroic tunnel junctions [1–4]. Optimally doped manganite $La_{0.67}Sr_{0.33}MnO_3$ (LSMO) is one of the most interesting candidates for electronic devices based on its metal–semiconductor transition property [5–8]. Many reports focused on the transport properties of LSMO films under magnetic field and low temperature [6, 9–11]. Current–voltage (*I–V*) characteristics of epitaxial LSMO films deposited on Nb-doped $SrTiO_3$ substrates show rectifying behavior, which also was reported [4, 9]. Nb-doped $SrTiO_3$ single crystals are good candidates used as conductive substrates to prepare LSMO films due to the well-fitted lattice parameters and low electrical resistivity.

LSMO films are also used to probe spin polarization at the $BaTiO_3$/Fe interface [12]. It is necessary to investigate the properties of leakage currents through the LSMO films for the applications of related electronic devices. The growth temperature and oxygen partial pressure can affect the structural and electrical properties of LSMO films, especially Curie temperature (T_C) [13]. Semi-conducting-like LSMO films ($T > T_C$) on NSTO substrates, which are heavily Sr-doped p-type semiconductor, also show rectifying *I–V* characteristic. In this paper we prepared such semi-conducting-like LSMO films on NSTO substrates by pulsed laser deposition method. The space-charge-limited conduction (SCLC), Schottky emission (S-E) and Fowler–Nordheim (F–N) tunneling mechanisms for the *I–V* curves of this kind of p–n junction under forward/backward bias are discussed, which is seldom reported for LSMO films. The changes of the barrier height and thickness near the interface of p–n junctions are considered to explain such *I–V* properties.

Published online: 13 March 2014

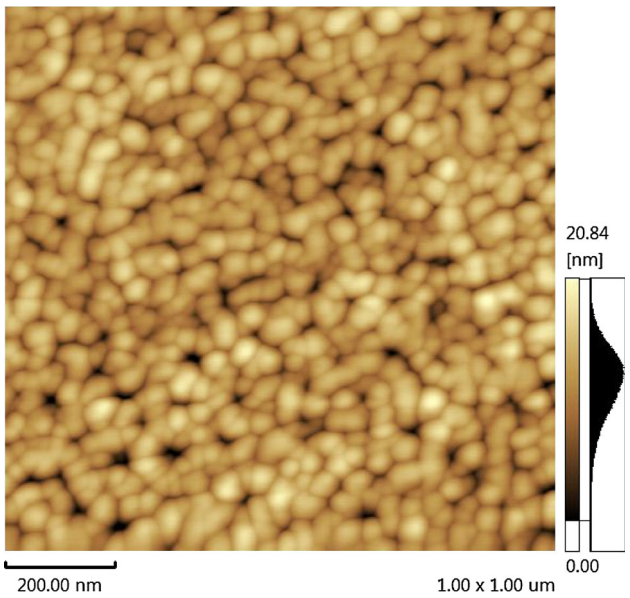

Fig. 1 1 × 1 μm AFM image of the surface of the LSMO film

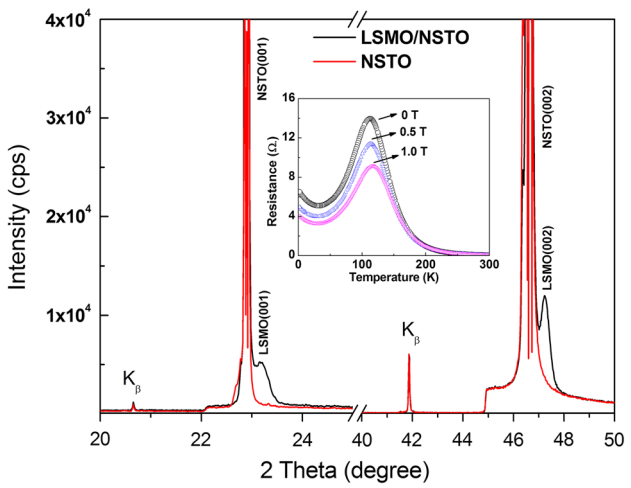

Fig. 2 The XRD pattern of the LSMO films grown on the NSTO substrates, *inset* shows temperature-dependent resistance of the LSMO films with and without a magnetic field applied in the in-plane direction of LSMO films

2 Experimental

LSMO thin films were prepared on NSTO (001) single-crystal substrates at 700 °C using the pulsed laser deposition technique. The electrical resistivity of the NSTO substrates is about 7.0 mΩ·cm at room temperature, which were chemically cleaned and annealed at 1,100 °C for 10 h in air before the deposition to get atomically smooth surface [14]. A KrF excimer laser (the wavelength is 248 nm) operating at 2 J/cm^2 was focused on the surface of a rotating powder target at a 45° angle of incidence. NSTO substrates were placed on a heater, which was 50 mm away from the target. The working pressure during the depositing was maintained at 1.0 Pa by O_2 flow rate. As-prepared LSMO/NSTO samples were annealed in a tube furnace in air.

The surface quality of the LSMO films was examined by an atomic force microscopy (AFM: Shimadzu, SPM-9700). The resistance was measured by a normal four-probe technique using a commercial physical property measurement system (PPMS: Quantum Design). The crystalline structure of the obtained LSMO films was analyzed by an X-ray diffractometer (XRD: RIGAKU, D/MAX-RB) with CuKα radiation ($\lambda = 0.15405$ nm).

I–V characteristic measurements were performed by a ferroelectric parameter test system (RT, Precision Premier II) at room temperature. Before each measurement, Indium electrodes (about 0.1 mm^2) were pressed on the films and substrates to get Ohmic contact, respectively. To avoid exceeding the limit current of the measurement system, the highest bias voltage is limited to 1.5 V.

3 Results and discussion

AFM image in Fig. 1 shows that the LSMO films had smooth surface morphology and are strongly oriented on the NSTO (001) substrates. The typical thickness of the films is about 100 nm. XRD patterns displayed in Fig. 2 show that LSMO phase is pseudo-cubic phase. Only (00*l*) diffraction peaks are presented, which indicates an epitaxial growth of the LSMO films on the NSTO (001) substrates.

The *inset* of Fig. 2 gives the resistivity-temperature relationship of the prepared LSMO films, which shows a clear transition from metallic-like to semi-conducting-like below 100 K due to the low oxygen partial pressure during the film depositing. Literatures also report that the maximum electrical resistivity of LSMO films decreases shifts towards higher temperature with the increasing of the oxygen partial pressure [9, 13].

Figure 3 shows *I–V* curves of the In/LSMO/NSTO/In structure in semi-log scale. *I–V* curves of LSMO/NSTO under forward and reverse bias clearly demonstrate a rectifying behavior, which is similar with other reports [4, 9]. The *logI–V* curves of the In/LSMO/NSTO/In structure in Fig. 3 depart substantially from the thermionic-emission theory. For the thermionic-emission theory, *logI–V* curve is almost linear, especially at room temperature [15, 16]. So there are other mechanisms for the leakage currents of our prepared LSMO/NSTO junctions as following discussed.

Ohmic conduction mechanism is described for a linear current–voltage curve $I \propto V$, which usually occurs under very low bias with the presence of free charge-carriers in materials [17, 18]. According to SCLC model, a linear dependence $I \propto V$ under lower voltage corresponds to the

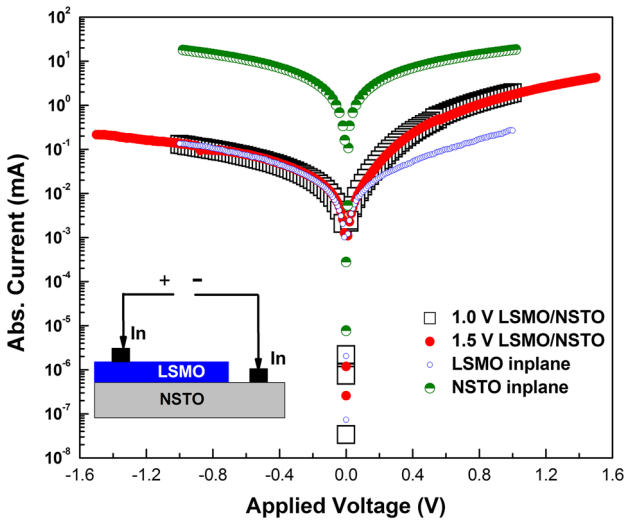

Fig. 3 *I–V* curves in semi-log scale for the In/LSMO/NSTO/In structure. Maximum voltages are 1.0 V (*open square*) and 1.5 V (*solid circle*), respectively. The *inset* shows the measurement schematic of a conventional sandwiched structure (not to scale). For *I–V* curves of LSMO in-plane (*open circle*) and NSTO in-plane (*semi circle*), two-probe configuration was used

Ohmic law region. At higher voltages, the current follows a square dependence on voltage: $I \propto V^2$, which corresponds to the Child's law region [19]. For Schottky emission, the *I-V* relationship can be written as following [20, 21],

$$\ln I \propto \sqrt{V}.\frac{e^3}{4\pi\varepsilon_0\varepsilon_r d}\Big/kT \tag{1}$$

where I is the current, V is the applied voltage, e is the electronic charge, k is the Boltzmann's constant, $\varepsilon_r\varepsilon_0$ is the dielectric constant and d is the thickness of the barrier. Giving the same film thickness and same temperature, Eq. (2) can be written as $\ln I \propto V^{1/2}$. For F–N tunneling, the formula can be written as [22–24],

$$J = AE^2 \exp\left(-\frac{B}{E}\right) \tag{2}$$

where J is the current density and E is the electric field. Both A and B are parameters related with the electron mass and the barrier height. There is a relationship between parameter B and the barrier height ϕ_B, $B \propto \phi_B^{3/2}$. Here we can rewrite Eq. (2) as $I/V^2 \propto \exp(-B/V)$ for the same film. Then we can distinguish the conduction mechanism from others by considering the slopes of *I–V* curves in the log–log scale (see Fig. 4). To exclude the effects of the interfaces between In electrodes and the substrates or films, *I–V* curves of In/NSTO/In and In/LSMO/In structures were also measured. The slopes of log*I*–log*V* curves of LSMO in-plane or NSTO in-plane are nearly 1.0 under the whole voltage measured and indicate that In electrodes are Ohmic contacted with NSTO substrates or LSMO films.

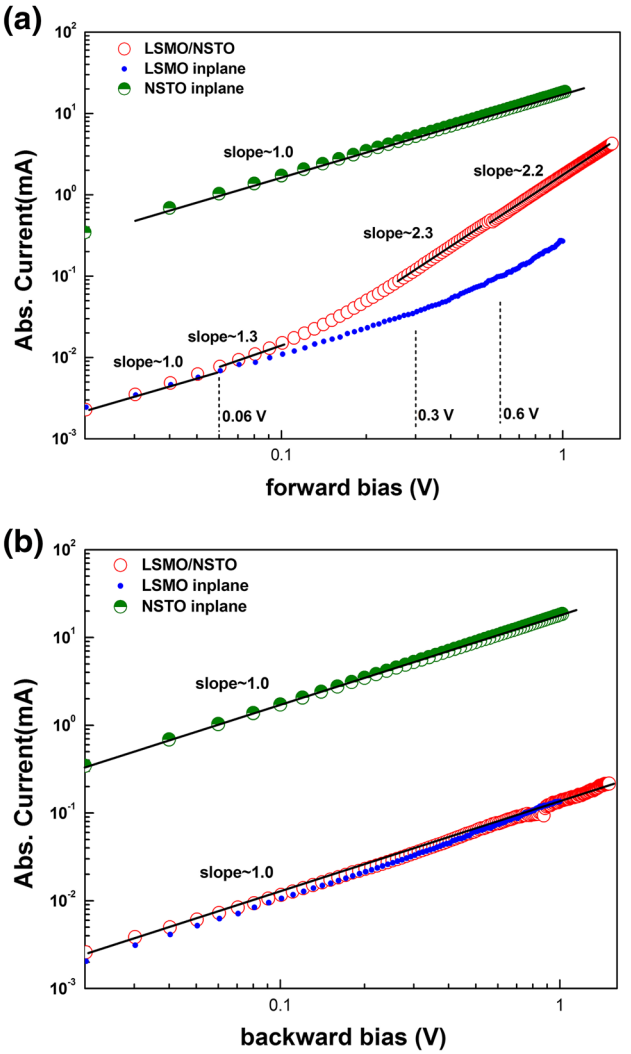

Fig. 4 *I–V* curves of LSMO/NSTO (*open circle*), LSMO in-plane (*solid circle*) and NSTO in-plane (*semi circle*) in log–log scale under: **a** forward bias, **b** backward bias

At low voltage ($V < 0.06$ V, which is the order of kT/e voltage [25]), due to the high density of free charge-carriers inside LSMO film and NSTO substrate, *I–V* curves in Fig. 4 under forward or backward bias exhibit the linear behavior, corresponding to the Ohmic law region of SCLC model. It can be noted that such current is not diffusion current but the drift current [18]. There are high density of free charge-carriers such as holes in the LSMO film and electrons in the NSTO substrate. They can be drifted for the application of voltages. Because of high and wide barrier of the interface of the LSMO/NSTO under low bias [5, 7], injected/tunneling current can be neglected. It can be noted that such *I–V* curves are not the results of the generation-recombination process or high-injection condition because latter two processes show nonlinear *I–V* relationships [15].

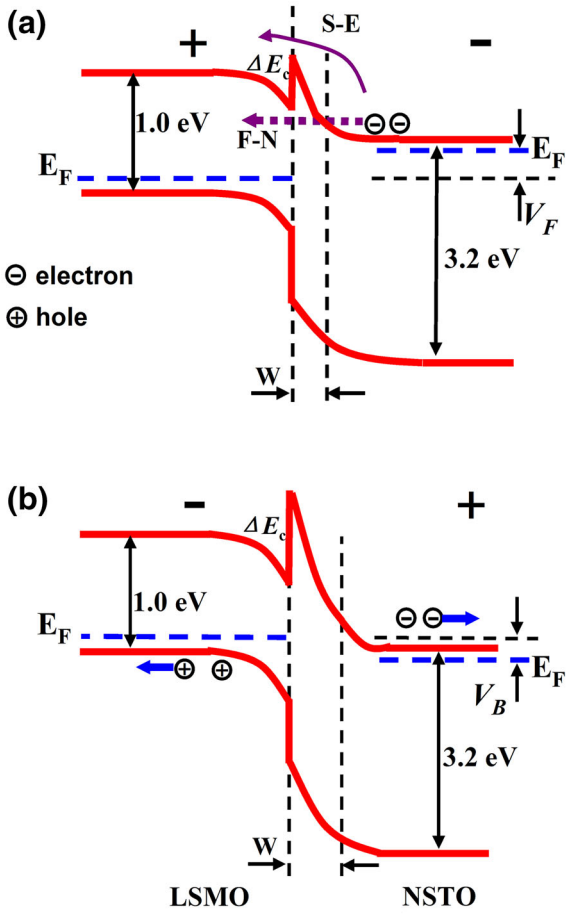

Fig. 5 Schematic band diagrams of the LSMO/NSTO junction under: **a** forward bias voltage V_F, **b** backward bias V_B

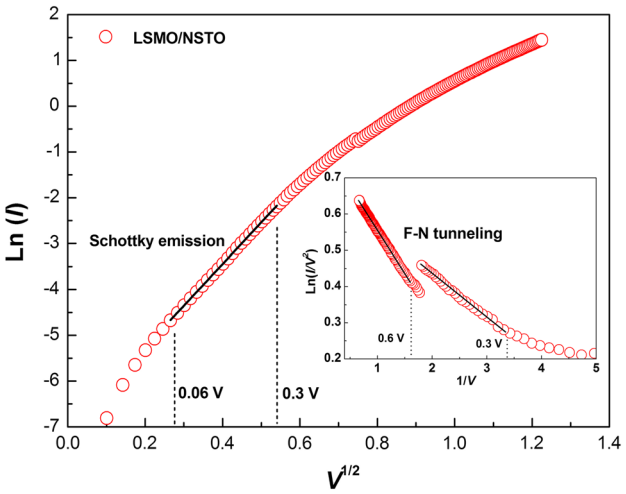

Fig. 6 Plots of Ln(I)–$V^{1/2}$ show the Schottky emission under the forward bias 0.06–0.3 V. *Inset*: plots of Ln(I/V^2)–1/V show the F–N tunneling under the forward bias exceeds 0.3 V

As the backward bias increases, the barrier becomes wide and even higher [9, 15]. Injected current or tunneling current is still neglected. So the slope of I–V curve under backward bias remains about 1.0 (see Fig. 4b). To get the Child's law region of SCLC, higher backward bias should be added. Similarly, as the forward bias increases from 0.06 V, neither can the Child's law region of SCLC be obviously seen (see Fig. 4a).

The energy-band diagrams at the interface of the LSMO/NSTO junction are shown in Fig. 5. The LSMO/NSTO junction we prepared is an anisotype heterojunction. There are different work functions for LSMO and NSTO (4.8 and 4.0 eV, respectively) [1]. LSMO has smaller band gap (about 1.0 eV) and it is p-type [26]. NSTO has bigger band gap (about 3.2 eV) and it is n-type [27].The conduction-band edge E_C goes through a peak near the junction, which is a triangular barrier for electrons. The difference in energy of the conduction-band edges in the two semiconductors is represented by $\triangle E_C$, here choosing $\triangle E_C$ as the barrier height [15]. The barrier's width w and height $\triangle E_C$ can be modulated by the applied bias. When a forward bias is added, the barrier of the LSMO/NSTO interface becomes narrower and lower (see Fig. 5).

The fittings of the measured I–V curves in Fig. 6 confirm the above-mentioned energy-band diagrams. Fig. 6 shows that the fitting lines are very close to the according curves under different bias voltages. The current increases with the increasing of the forward bias because of the narrowing and lowing of the barrier. The slopes of $logI$–$logV$ curves shift from about 1.1 to about 2.2 in Fig. 4a. We can see that Schottky emission occurs as the forward bias rises from 0.06 to 0.3 V.

When the forward bias increases more, the barrier becomes even thinner. Then the interface-limited F–N tunneling occurs above 0.3 V (see the *inset* in Fig. 6). The interface-limited F–N tunneling can make a substantial contribution toward the leakage currents at a higher bias, which has been reported [28]. For both LSMO films and NSTO substrates have high carrier densities, a several-nanometer-thick depletion region can form at the junction [9]. For heavily-doped NSTO and LSMO, the carrier concentrations calculated are 2.3×10^{20} and 1.65×10^{21} cm^{-3}, respectively [16]. According to the following defining [7, 15],

$$E_{00} \equiv \frac{q\hbar}{2}\sqrt{\frac{N}{m^* \varepsilon_s}} \tag{3}$$

we get that $E_{00} \approx 30$ meV for LSMO comparing with 0.01 wt% Nb:$SrTiO_3$ [7]. E_{00} is nearly the same order of k_BT (25 meV) at room temperature. So thermionic-field emission can occur at room temperature. The *inset* in Fig. 6 also shows that the slope of I/V^2–$1/V$ curve increases as the forward bias increases from 0.3 to 0.6 V, which is consistent with Eq. (2) because higher forward bias causes lower barrier height.

4 Conclusions

LSMO/NSTO p–n junctions were prepared, which leakage currents show rectifying property. At lower forward/backward bias, leakage currents follow the Ohmic law region of SCLC model. Schottky emission occurs then F–N tunneling mechanism as increasing the forward bias, which can be attributed to the narrowing and lowing of the interface barrier. Under the backward bias of the whole voltage measured, leakage currents remain the Ohmic law region of SCLC model, which is the drift currents of holes in the LSMO films and electrons in the NSTO substrates because of the widening and increasing of the barrier.

Acknowledgments We are grateful to the National Natural Science Foundations of China (Nos. 51272072, 61274010 and 51202062) and Program for New Century Excellent Talents Ministry of Education of China (NCET-09-0135).

References

1. M. Minohara, I. Ohkubo, H. Kumigashira, M. Oshima, Appl. Phys. Lett. **90**, 132123 (2007)
2. G. Srinivasan, E.T. Rasmussen, A.A. Bush, K.E. Kamentsev, V.F. Meshcheryakov, Y.K. Fetisov, Appl. Phys. A **78**, 721 (2004)
3. M. Hambe, A. Petraru, N.A. Pertsev, P. Munroe, V. Nagarajan, H. Kohlstedt, Adv. Func. Mater. **20**, 2436 (2010)
4. G. Kim, D. Mazumdar, A. Gupta, Appl. Phys. Lett. **102**, 052908 (2013)
5. Y.W. Xie, J.R. Sun, D.J. Wang, D.F. Guo, B.Y. Liang, B.G. Shen, J. Phys. D Appl. Phys. **42**, 185008 (2009)
6. D. Liu, W. Liu, Ceram. Inter. **37**, 3531 (2011)
7. K.G. Rana, S. Parui, T. Banerjee, Phys. Rev. B **87**, 085116 (2013)
8. M. Grobosch, K. Dörr, R.B. Gangineni, M. Knupfer, Appl. Phys. A **95**, 95 (2009)
9. C.Y. Lam, K.H. Wong, J. Eur. Ceram. Soc. **25**, 2141 (2005)
10. R. Bertacco, S. Brivio, M. Cantoni, A. Cattoni, D. Petti, M. Finazzi, F. Ciccacci, Appl. Phys. Lett. **91**, 102506 (2007)
11. X.W. Wang, Y.Q. Zhang, X. Wang, Z.J. Wang, Y.L. Zhu, Z.D. Zhang, Thin Solid Films **545**, 241 (2013)
12. V. Garcia, M. Bibes, L. Bocher, S. Valencia, F. Kronast, A. Crassous, X. Moya, S. Enouz-Vedrenne, A. Gloter, D. Imhoff, C. Deranlot, N.D. Mathur, S. Fusil, K. Bouzehouane, A. Barthélémy, Science **327**, 1106 (2010)
13. S. Maity, A. Dhar, S.K. Ray, D. Bhattacharya, J. Phys. Chem. Solids **72**, 804 (2011)
14. T. Yoshimura, N. Fujimura, T. Ito, J. Cryst. Growth **174**, 790 (1997)
15. S.M. Sze, *Physics of Semiconductor Devices*, 3rd edn. (Wiley, New York, 2006)
16. A. Ruotolo, C.Y. Lam, W.F. Cheng, K.H. Wong, C.W. Leung, Phys. Rev. B **76**, 075122 (2007)
17. M.A. Lampert, Rept. Prog. Phys. **27**, 229 (1964)
18. H. Goronkin, J. Appl. Phys. **38**, 4547 (1967)
19. W. Schottky, Naturwissenschaften **26**, 843 (1938)
20. H. Schroeder, S. Schmitz, P. Meuffels, Appl. Phys. Lett. **82**, 781 (2003)
21. V.M. Voora, T. Hofmann, M. Brandt, M. Lorenz, M. Grundmann, N. Ashkenov, M. Schubert, Appl. Phys. Lett. **94**, 142904 (2009)
22. R.H. Fowler, L. Nordheim, Proc. R. Soc. A **119**, 173 (1928)
23. Y.L. Chiou, J.P. Gambino, M. Mohammad, Solid State Electron. **45**, 1787 (2001)
24. X.S. Fang, L.F. Hu, K.F. Huo, B. Gao, L.J. Zhao, M.Y. Liao, P.K. Chu, Y. Bando, D. Golberg, Adv. Funct. Mater. **21**, 3907 (2011)
25. H.F. Tian, J.R. Sun, H.B. Lu, K.J. Jin, H.X. Yang, H.C. Yu, J.Q. Li, Appl. Phys. Lett. **87**, 164102 (2005)
26. K. Zhao, K.J. Jin, H.B. Lu, Y.H. Huang, Q.L. Zhou, M. He, Z.H. Chen, Y.L. Zhou, G.Z. Yang, Appl. Phys. Lett. **88**, 141914 (2006)
27. Z. Luo, P.K.L. Chan, K.L. Jim, C.W. Leung, Phys. B **406**, 3104 (2011)
28. J.G. Wu, J. Wang, D.Q. Xiao, J.G. Zhu, Mater. Res. Bull. **46**, 2183 (2011)